Chemistry

Physical & Theoretical Chemistry fields

Okayama University *Year* 2005

Infrared spectra of seeded hydrogen clusters: (para-H2)N-N2O and (ortho-H2)N-N2O, N=2-13

Jian Tang* Robert A. McKellar Dr.†

*Okayama University, jtang@cc.okayama-u.ac.jp

†Steacie Institute for Molecular Science

Infrared spectra of seeded hydrogen clusters: $(para\text{H}_2)_N$-N_2O and $(ortho\text{H}_2)_N$-N_2O, N = 2 to 13

Jian Tang* and A.R.W. McKellar

Steacie Institute for Molecular Sciences

National Research Council of Canada

Ottawa, Ontario K1A 0R6, Canada

ABSTRACT

High resolution infrared spectra of clusters containing *para*H_2 and/or *ortho*H_2 and a single nitrous oxide molecule are studied in the 2225 cm^{-1} region of the ν_1 fundamental band of N_2O. The clusters are formed in pulsed supersonic jet expansions from a cooled nozzle and probed using a tunable infrared diode laser spectrometer. The simple symmetric rotor type spectra generally show no resolved *K*-structure, with prominent *Q*-branch features for *ortho*H_2 but not *para*H_2 clusters. The observed vibrational shifts and rotational constants are reported. There is no obvious indication of superfluid effects for *para*H_2 clusters up to N = 13. Sharp transitions due to even larger clusters are observed, but no definite assignments are possible. Mixed $(para\text{H}_2)_N$-$(ortho\text{H}_2)_M$-N_2O cluster line positions can be well predicted by linear interpolation between the corresponding transitions of the pure clusters.

I. INTRODUCTION

Recently it has been shown that high resolution infrared spectra can be observed and assigned for small helium atom or hydrogen molecule clusters containing a single chromophore molecule. So far, helium clusters are more thoroughly studied, with a number of chromophores being utilized (OCS, N_2O, CO_2, and CO)[1-7], and analogous microwave spectra also being detected in some cases. It is thus possible to extend previous helium nanodroplet isolation spectroscopy (HENDI) results[8-10] which involved cluster sizes of $N \approx 10^3$ to 10^4, to the regime of small clusters with $N \approx 2$ to 20.

In the case of hydrogen clusters, we previously reported spectra of $(para\text{H}_2)_N$-CO with N = 2 to 14,[11] and of $(para\text{H}_2)_N$-, $(ortho\text{H}_2)_N$, and $(\text{HD})_N$-OCS with N = 2 to 7.[12] In general, it

* Current address: Department of Chemistry, Faculty of Science, Okayama University, 3-1-1 Tsushima-naka, Okayama 700-8530, Japan.

has proven more difficult to pursue spectroscopic observations to larger *N*-values with hydrogen than with helium. But hydrogen introduces novel aspects to these cluster studies, such as the availability of different forms (*para*H_2, *ortho*H_2, HD, etc.), the presence of unquenched rotational angular momentum for *ortho*H_2, the possibility of observing mixed clusters (containing various forms of hydrogen and/or helium), and even the possible chance of observing superfluid effects in finite size *para*H_2 clusters.[13,14] A further reason for interest in hydrogen clusters is the possibility of comparisons with matrix isolation spectra obtained with solid hydrogen.[15]

For (hydrogen)$_N$-OCS, simple symmetric rotor type spectra without resolved *K*-structure were observed.[12] Prominent *Q*-branch features were present for *ortho*H_2 and HD, but absent for *para*H_2. The vibrational shifts and rotational parameters continued trends previously observed[16] for the binary complexes (with $N = 1$), but there was no evidence for decoupling of the rotational motion, as observed in He clusters,[5-7] which could be attributed to the onset of superfluid behavior. The present paper reports infrared spectra of (hydrogen)$_N$-N_2O clusters, as observed in the 2225 cm^{-1} region of the ν_1 fundamental band of N_2O. Since OCS and N_2O are members of the same 'carbon dioxide molecular family,' the present results are somewhat similar to those of Ref. 12, for example the absence/presence of strong *Q*-branch features for *para*H_2/*ortho*H_2. Fortunately, in the present case it has been possible to detect spectra for larger clusters, especially for (*para*H_2)$_N$-N_2O where assignments are possible up to about $N = 13$ and lines can still be observed up to $N \approx 20$.

H_2 is lighter than He, but intermolecular forces involving H_2 are usually stronger, so that quantum effects tend to be less significant in hydrogen clusters. Nevertheless, the hunt for possible superfluidity in *para*H_2 clusters has motivated a number of recent experiments[1417-19] involving (hydrogen)$_N$–OCS clusters embedded within He nanodroplets and corresponding calculations.[20-22] Helium nanodroplets have also been used[19] to isolate small $(HD)_N$ – HCN clusters. Pure hydrogen clusters are of considerable interest, but more difficult to observed spectroscopically: infrared spectra of hydrogen dimers, $(H_2)_2$, are well known,[24] calculations on hydrogen trimers, $(H_2)_3$, have been reported,[25] and larger clusters have recently been observed by Raman spectroscopy.[26]

Hydrogen molecules have two nuclear spin states, *para* with resultant spin zero, and *ortho* with resultant spin one. Symmetry allows only even values of rotational angular momentum for *para*H_2, and only odd values for *ortho*H_2. In the present experiment, all *para*H_2 molecules have $J = 0$, and all *ortho*H_2 have $J = 1$, because the effective rotational temperature is low (< 1 K). This rotational quantum number tends to remain 'good' even in a cluster, that is, H_2 rotates almost freely. So *para*H_2 molecules are effectively spherical. At room temperature, normal H_2 is composed of 25% *para* and 75% *ortho* and this ratio persists in a supersonic expansion, since spin conversion is slow. However, it is relatively easy to prepare almost pure *para*H_2 in the laboratory, as we have done here.

II. RESULTS

A. Experimental details

The apparatus has been described previously.[2,4,27] A pulsed supersonic expansion was probed by a tunable diode laser operating in a rapid-scan signal averaging mode. A room temperature N_2O gas cell and temperature-stabilized solid Ge etalon were used for

wavenumber calibration. Slit- and pinhole-shaped orifices were used with the cooled jet nozzle, the slit giving sharper spectral lines and the pinhole giving lower temperatures and more clustering. The expansion gas mixture was mostly helium with 1 to 3% hydrogen and <0.01% N_2O. *Para*H_2 was prepared in batches by liquefying hydrogen in the presence of a catalyst, and then mixed with the other gases as described previously.[11,12]

B. (*para*H_2)$_N$ – N_2O clusters

The starting point of this work was our previous results for H_2-N_2O complexes,[16] where distinct, but similar, spectra were observed for *para*H_2-N_2O and *ortho*H_2-N_2O. These were analyzed as *a*-type (ΔK_a = 0) transitions of an asymmetric rotor with a T-shaped structure, effective intermolecular separations of about 3.4 Å, and angles of about 80° between the NNO and intermolecular axes. By cooling the jet nozzle and going to higher backing pressures than used in Ref. 16, additional lines due to larger clusters started to appear, as illustrated in Fig. 1. Here the lower three traces are slit jet spectra (narrower lines, higher effective temperature), the upper three traces are pinhole jet spectra (broader lines, more clustering), and within each group the traces are arranged in order of increasing backing pressure. In the lowest pressure slit jet trace, almost all the features are known lines of N_2O (marked 0 *R*(0) and 0 *R*(1), where the first digit is *N*, the number of H_2 molecules), of *para*H_2-N_2O (marked 1, or 1 *R*(0), etc.), and of *ortho*H_2-N_2O (marked 1#). These lines of *ortho*H_2-N_2O appear even though almost pure (>99%) *para*H_2 was used here. This is a manifestation of the fact that *ortho*H_2-N_2O complexes are more strongly bound and tend to form preferentially in the competitive supersonic jet environment. Judging by the relative strengths of the *R*(0) lines of the two *N* = 1 species, our *para*H_2 purity was somewhat better here than previously (cf. Fig. 1 of Ref. 16).

Even in the bottom trace of Fig. 1, a couple of weak new lines also appear which can readily be assigned as *R*(0) of (*para*H_2)$_2$-N_2O and (*para*H_2)$_3$-N_2O (marked 2*R*(0) and 3*R*(0)). As the pressure is increased further, additional lines appear due to larger clusters, with assignments as indicated. The 4*R*(0) and 5*R*(0) lines are almost coincident, so that they are not easily resolved in the pinhole jet spectra. But fortunately they can be clearly distinguished in the slit jet spectra. The series turns around and there is then a rather large gap before 6*R*(0) appears (this was also the case for (*para*H_2)$_N$-OCS),[12] followed by 7*R*(0) and 8*R*(0) moving to lower wavenumbers. There is a complication for 6*R*(0) in that the single moderate-strength line in the pinhole jet spectra appears to fragment into a number of components in the better-resolved slit jet spectra. This point is discussed further in Sec. III.A. below.

The further evolution of the spectrum with increased clustering is shown in Fig. 2. This and subsequent figures were recorded with a partly-skimmed pinhole nozzle arrangement (not yet optimized) which combines some of the advantages of the pinhole and slit configurations. The assigned *R*(0) features for *N* = 8 - 11 are quite evenly spaced, although 9 and 10 are weaker and 10 is somewhat overlapped by other lines. Subsequently, the *R*(0) lines marked 11, 12, and 13 are stronger and more clearly resolved. Overall, the assignments up to this point are reasonably unambiguous, though of course this judgment requires very careful examination of these and many other spectra. Most of the strong and medium features in the spectra can be explained, and virtually all expected lines can be accounted for (though they may be obscured by stronger lines). The collected assignments for (*para*H_2)$_N$-N_2O clusters are listed in Table I.

What about even larger clusters, with $N > 13$? Figure 3 shows the results of moving to higher backing pressures with a cold (-92 C) nozzle. Another regularly spaced line appears which we can assign to 14 $R(0)$, but then about 8 to 10 lines appear with little apparent regularity in the region from 2223.0 to 2223.3 cm^{-1}, including a particularly prominent one at 2223.243 cm^{-1}. Finally, in the top traces of Fig. 3, further clustering is manifested by the disappearance of these sharper lines and the appearance of a strong broad feature centered at about 2223.10 cm^{-1} with an overall width of about 0.2 cm^{-1}. Interestingly, some residual structure (widths ≈ 0.01 cm^{-1}) persists on the broad peak. There also seems to be a weaker, but equally broad feature centered at about 2223.48 cm^{-1}. Spectra recorded in the region below 2222.8 cm^{-1} (not shown here) show no further structure. So we can speculate that $(para H_2)_N$-N_2O clusters have a reasonably regular spectral structure up to about $N = 15$, followed by a range from about $N = 15$ to 25 where the $R(0)$ lines are still sharp (<0.004 cm^{-1}) but their positions are irregular. Then for N greater than about 25 the $R(0)$ lines become broader (or at least so closely spaced that they are not resolved) and mostly coalesce around 2223.1 cm^{-1}. Further discussion of larger clusters is given in Sec. III.C. below.

C. $(ortho H_2)_N$ – N_2O clusters

We knew[16] that the binary $ortho H_2$-N_2O complex exhibits a larger vibrational shift (+0.624 cm^{-1}) than does $para H_2$-N_2O (+0.226 cm^{-1}). Thus we expected the first few $R(0)$ lines of $(ortho H_2)_N$-N_2O to spread out considerably more than those of $(para H_2)_N$-N_2O, since these lines tend to form a regular series for $N = 1$ to 4 or 5. This was indeed the case, as is shown in Fig. 4 which was obtained using normal H_2 in the expansion gas mix, in contrast to Figs. 1-3, obtained with almost pure $para H_2$. For $ortho H_2$-N_2O, the $R(0)$ line lies 0.455 cm^{-1} above that of N_2O itself. The next prominent pressure-sensitive line occurs a further 0.495 cm^{-1} higher in wavenumber, and was assigned as 2 $R(0)$; subsequent N $R(0)$ lines were assigned with further blue shifts of 0.560, 0.567, and 0.231 cm^{-1} (see Fig. 4). Based on $(H_2)_N$-OCS spectra,[12] we also expected, and indeed found, Q-branch features and $R(1)$ lines to be more prominent with $ortho H_2$ clusters than with $para H_2$, particularly for larger N-values (> 3). For example, in Fig. 4 the features marked 5 Q and 5 $R(1)$ are almost the same strength as 5 $R(0)$. This difference between *ortho* and *para* clusters is a nuclear spin statistical effect, as discussed below.

The measured wavenumbers of the $(ortho H_2)_N$-N_2O cluster transitions are listed in Table II. We consider there assignments to be fairly reliable up to and including $N = 6$. For $N = 7$ (not shown in Fig. 4), they are less certain, but seem quite reasonable; one difficulty is that each of the $N = 7$ lines is only partly resolved from a stronger neighbor. We did not observe any evidence for larger $ortho H_2$ clusters.

D. Mixed clusters

We observed a considerable number of features which could be assigned to mixed $(para H_2)_N$-$(ortho H_2)_M$-N_2O clusters. Some of these were apparent even when using fresh $para H_2$ in the expansion gas mixture, as the outnumbered but stickier $ortho H_2$ molecules attempted to dominate, and others were apparent when using normal H_2. We also made systematic investigations by adding small amounts of normal H_2 to $para H_2$ samples in order to help to confirm and extend the assignments.

As an example, Table III lists the $R(0)$ transitions of all possible mixed clusters with $(N + M) = 2$ to 5. A few of these mixed cluster lines are visible in Figs. 1 and 4, where they are

marked ‘m’. The positions of the mixed cluster lines were observed to fall very close to what is expected by linear interpolation between the $R(0)$ transitions of the corresponding pure clusters, as already noted for OCS clusters.[12] This is shown in the last column of Table III. For cluster size $(N + M) = 5$, we noted a small systematic variation from this linearity, with the residuals (obs − calc) in Table III being equal to +0.012, +0.020, +0.021, +0.013 cm^{-1} for the clusters with $(N, M) = (4,1), (3,2), (2,3)$, and $(1,4)$, respectively.

Some transitions other than $R(0)$ were also observed for the mixed clusters, but we do not have enough of these for a detailed analysis. The problem is that we rapidly reach a ‘confusion limit’ due to the overlapping of lines and the dilution of intensity from the abundance of possible mixed species.

III. ANALYSIS and DISCUSSION

A. Nature of the spectra

As in the case of $(H_2)_N$-OCS,[12] the present *para*H_2 clusters do not exhibit prominent Q-branch features. In contrast, the strong Q features observed in the *ortho*H_2 spectra indicate the presence of higher K-values. The difference between the *para* and *ortho* clusters is due to nuclear spin statistics. Briefly, most *para*H_2 clusters are in $K = 0$ levels, for which Q-branches are not allowed, because energetically accessible $K \neq 0$ states are symmetry-forbidden due to the zero resultant nuclear spin of *para*H_2. The relative intensities of the various observed transitions are very different for the *para* and *ortho* clusters, but they follow closely the trends observed for $(H_2)_N$-OCS and can be explained in exactly the same terms (see Sec. III.B. of Ref. 12).

Clusters with $N = 2$ are a special case, since they must be asymmetric rotors. We noted the presence of some broad unresolved structure around 2224.2 cm^{-1} which may be due to Q-branch transitions of $(para H_2)_2$-N_2O – this is indicated on Fig. 2. In the case of $(ortho H_2)_2$-N_2O, there is a Q-branch with some partly resolved structure (see Fig. 4), and moreover there may be substructure on the $R(0)$ and $R(1)$ transitions (satellite features at 2225.524 and 2226.025 cm^{-1}, respectively, also apparent in Fig. 4). In the simpler case of He_2-N_2O it has recently been possible to make a detailed experimental and theoretical energy-level analysis;[28] we can expect that a similar detailed analysis should be possible for $(H_2)_2$-N_2O in the future.

As mentioned above, the $(para H_2)_6$-N_2O cluster posed a problem in that its $R(0)$ transition, which was a single line in pinhole jet spectra (colder but lower resolution), seemed to split into two or more weaker components in slit jet spectra. It was difficult to tell whether this was also the case for other transitions of $(para H_2)_6$-N_2O since they were weak at best and sometimes obscured by other lines. The apparent splitting of $R(0)$ could be an artifact of spectral resolution, that is, the same components were present in the pinhole spectrum, but just not resolved. Or it could be a real effect of temperature, that is, very low-lying energy levels became populated in the warmer slit jet spectrum, leading to multiple $R(0)$ lines. Experimentally, the latter possibility seems more likely, but it is difficult to be sure. Either way, we speculate that $N = 6$ may also be a special case, in which a single H_2 molecule has been added to a stable “core” (namely the $N = 5$ cluster, with its filled donut ring – see below). In this “core plus single particle” model, the $N = 6$ cluster is more likely to act like an asymmetric rotor (for example, with distinct *a*- and *b*-type $R(0)$ transitions) and/or more likely to have very low frequency vibrational modes (which would be populated in the slit jet, but not pinhole jet, spectra).

B. Fitted parameters

Due to the very simple nature of most of the spectra (no resolved *K*-structure) it was possible to analyze them using a simple linear molecule energy level expression, $E(J) = \nu_0 + B\,J(J+1) - D\,[J(J+1)]^2$. Table IV shows the results of fitting this expression to the line position data of Tables I and II. These parameters are mainly intended for purposes of intercomparison, rather than detailed analysis, since (for one thing) we know little about the detailed rotational energy level structure of these clusters. Thus in most cases the upper and lower state *B*-values were constrained to be equal, and the parameter uncertainties are not quoted here (these would be almost meaningless because of the limited data and our ignorance of the true Hamiltonian).

The variation in the band origins for the $(H_2)_N$-N_2O clusters from Table IV is illustrated in Fig. 5, which also shows for comparison the data for He_N-N_2O.[5] For N = 1 to 4, the hydrogen (and helium) clusters show an trend of almost linear vibrational blue shifts, though the magnitude of the shift is more than twice as large for *ortho*H_2 as for *para*H_2 and He. Then in going from N = 4 to 5, there are significant reductions in the shift rate for *para* and *ortho*H_2 (more so for *para*), and only a slight reduction for He. For *para*H_2 and He the vibrational shift turns around in going from N = 5 to 6, and the trend is then uniformly negative. The same turnaround also happens for *ortho*H_2, but not until above 6. These vibrational shift trends can be explained by the 'donut' model, in which the first 5 or so H_2 molecules (or He atoms) form a ring around the N_2O in the energetically favored T-shaped configuration. When the ring is filled, the subsequent H_2 molecules must then occupy locations closer to the ends of the N_2O, where they have a net red shifting effect. The present results appear to indicate that 4 *para*H_2 molecules almost fill the donut ring, so that the ring diameter is forced to increase and/or the fifth hydrogen starts to spill out of it. In contrast, with $(He)_N$-N_2O clusters, 5 atoms are close to a perfect fit.[5] We can naively suggest that H_2 is larger than He, so that slightly fewer are able to fit into the donut. The behavior of *ortho*H_2 is similar, but the turnaround is less sharp. A possible rationalization for this is to note that the initial blue shift rate for *ortho*H_2 is so large that it simply takes longer to overcome it and finally begin the red shift.

The vibrational shifts observed previously[12] for $(hydrogen)_N$-OCS clusters are different than those seen here in that they are uniformly negative (i.e. red shifts). But there are also strong similarities, with an almost linear slope for N = 0 to 5, followed by a change to a more negative slope. In a further similarity, the $(ortho H_2)_N$-OCS clusters are always more blue shifted than $(para H_2)_N$-OCS (c.f. Fig. 5 of Ref. 12).

The variation of the rotational constant with cluster size is shown in Fig. 6. Both *para*H_2 and *ortho*H_2 clusters show a monotonic decrease in *B*, with the *ortho*H_2 *B*-values being uniformly somewhat smaller. This difference, also observed for $(H_2)_N$-OCS clusters,[12] means that an *ortho*H_2 cluster of a given size has a larger rotational moment of inertia than the corresponding *para*H_2 cluster. Thus the *ortho*H_2 molecules must be further away from the N_2O, even though they are more strongly bound to it (i.e. *ortho*H_2 is larger and stickier than *para*H_2). The monotonic decrease in *B* stands in contrast to $(He)_N$-N_2O clusters, where a turnaround in *B* is observed[5] for N > 6. The absence of a turnaround in Fig. 6 indicates that we have no obvious evidence for superfluid type behavior for $(para H_2)_N$-N_2O clusters. The *B*-value for $(para H_2)_5$-N_2O is a bit higher than would be expected on the basis of the remainder of the curve in Fig. 6. To a lesser extent, the same is true for $(ortho H_2)_5$-N_2O, and indeed for the (H_2)-OCS clusters[12] with N = 5. It is also evident in theoretical simulations of $(para H_2)_N$-

OCS.[23] We can take this as additional evidence for the special nature of the N = 5 clusters, with their filled donut ring. There is no room left in the ring for the sixth added H_2 molecule, which is forced to locate farther from the cluster center of mass, giving a larger increase in moment of inertia.

C. Larger *para*H_2 clusters (N > 10)

It is apparent from Fig. 3 that something happens to (*para*H_2)$_N$-N_2O as the cluster size reaches about 15 or 16. The vibrational shifting stops (or slows down), the regularity of the $R(0)$ line progressions ends, and the lines begin to broaden. Maybe these changes are related to the completion of the first solvation shell of *para*H_2 molecules around the N_2O. At this point, H_2-H_2 interactions would start to become more important than H_2-N_2O interactions. Different isomers might become possible, leading to fragmentation of the spectrum, and eventually the clusters might show crystalline, rather than liquid-like, characteristics. Alternately, the confusion around N = 15 could be a manifestation of an onset of superfluid effects: this explanation is supported by the very recent theoretical simulations of (*para*H_2)$_N$-OCS clusters by Paesani et al.,[23] which show a generally monotonic decrease in B-value with N except for a slight bump at N = 10 and a larger bump at N = 14, 15. The existence of a similar B-value bump in the present case could help to explain the break in the $R(0)$ series around N = 15.

Thinking in terms of the limit of very large N, a study of the spectrum of N_2O isolated in a *para*H_2 matrix would be very interesting for comparison with Fig. 3.

IV. CONCLUSIONS

In the face of the somewhat similar behavior of the *para*H_2 and *ortho*H_2 clusters, it is easy to forget that each *ortho*H_2 molecule has rotational angular momentum, J = 1. Most differences between *para* and *ortho* clusters can be explained by nuclear spin effects, not rotational angular momentum, as shown by spectra of (HD)$_N$-OCS.[12] We have previously posed the question of what "happens to" this angular momentum in *ortho*H_2-containing complexes or clusters, and we still don't have an answer. For some binary complexes like *ortho*H_2-N_2O, the angular momentum "mysteriously disappears" (in that the observed spectrum is similar to *para*H_2-N_2O),[16] whereas for others, like *ortho*H_2-CO_2, it "reappears" (the spectrum is very different from *para*H_2-CO_2).[29] In the case of a larger cluster like (*ortho*H_2)$_7$-N_2O, it is daunting to try to imagine the fate of all those J = 1 angular momentum vectors!

This paper has reported high resolution infrared spectra of hydrogen clusters seeded with a single nitrous oxide chromophore molecule. These spectra accompany the ν_1 fundamental band of N_2O near 2225 cm^{-1}, and were recorded using a rapid-scan tunable diode laser system to probe a pulsed supersonic jet expansion. Cluster sizes up to N = 7 for (*ortho*H_2)$_N$-N_2O, and up to N = 13 for (*para*H_2)-N_2O, were analyzed, and even larger *para*H_2 cluster transitions were readily apparent but not easily assigned. The observed spectra generally had a very simple P-, Q-, R-branch structure, with prominent Q features for *ortho*H_2 but not *para*H_2. Mixed clusters containing both *para*H_2 and *ortho*H_2 were also observed with line positions that could be accurately predicted by linear interpolation between those of the same-sized pure clusters. The derived vibrational band origins showed an initial blue shift up to N = 5 or 6, corresponding to filling of an equatorial "donut ring" around the N_2O, with a magnitude which was considerably greater for the *ortho*H_2 clusters. This was followed by a

red-shift as subsequent H_2 molecules were forced to locate closer to the ends of the N_2O. The derived rotational constants showed a monotonic decrease, with a slight kink at $N = 5$ giving evidence of this cluster's compact size and greater stability. Generally speaking, the present results are similar to those reported for $(H_2)_N$-OCS, and they bring us close to the region ($N \approx 15$) where certain superfluid effects are predicted[23] to become significant for *para*H_2 clusters.

REFERENCES

[1] J. Tang, Y. Xu, A.R.W. McKellar, and W. Jäger, Science **297**, 2030 (2002).
[2] J. Tang and A.R.W. McKellar, J. Chem. Phys. **119**, 754 (2003).
[3] Y. Xu and W. Jäger, J. Chem. Phys. **119**, 5457 (2003).
[4] J. Tang and A.R.W. McKellar, J. Chem. Phys. **119**, 5467 (2003).
[5] Y. Xu, W. Jäger, J. Tang, and A.R.W. McKellar, Phys. Rev. Lett. **91**, 163401 (2003).
[6] J. Tang, A.R.W. McKellar, F. Mezzacapo, and S. Moroni, Phys. Rev. Lett. **92**, 145503 (2004).
[7] J. Tang and A.R.W. McKellar, J. Chem. Phys. **121**, 181 (2004).
[8] J.P. Toennies and A.F. Vilesov, Ann. Rev. Phys. Chem. **49**, 1 (1998).
[9] See the special topic on helium nanodroplets, J. Chem. Phys. **115**, 10065-10281 (2001).
[10] C. Callegari, K.K. Lehmann, R. Schmied, and G. Scoles, J. Chem. Phys. **115**, 10090 (2001).
[11] S. Moroni, M. Botti, S. De Palo, and A.R.W. McKellar, J. Chem. Phys. **122**, 094314 (2005).
[12] J. Tang and A.R.W. McKellar, J. Chem. Phys. **121**, 3087 (2004).
[13] V.L. Ginzburg and A.A. Sobyanin, JETP Lett. **15**, 242 (1972).
[14] S. Grebenev, B. Sartakov, J.P. Toennies, and A.F. Vilesov, Science **289**, 1532 (2000).
[15] For example: T. Momose, M. Miki, T. Wakabayashi, T. Shida, M.-C. Chan, S.S. Lee, and T. Oka, J. Chem. Phys. **107**, 7707 (1997); H. Katsuki, T. Momose, and T. Shida, J. Chem. Phys. **116**, 8411 (2002); D.T. Anderson, R.J. Hinde, S. Tam, and M.E. Fajardo, J. Chem. Phys. **116**, 594 (2002).
[16] J. Tang and A.R.W. McKellar, J. Chem. Phys. **117**, 8308 (2002).
[17] S. Grebenev, E. Lugovoi B. Sartakov, J.P. Toennies, and A.F. Vilesov, Faraday Discuss. **118**, 19 (2001).
[18] S. Grebenev, B. Sartakov, J.P. Toennies, and A.F. Vilesov, Phys. Rev. Lett. **89**, 225301 (2002).
[19] D.T. Moore and R.E. Miller, J. Chem. Phys. **119**, 4713 (2003).
[20] Y. Kwon and K.B. Whaley, Phys. Rev. Lett. **89**, 273401 (2002).
[21] F. Paesani, R.E. Zillich, and K.B. Whaley, J. Chem. Phys. **119**, 11682 (2003).
[22] Y. Kwon and K.B. Whaley, J. Low Temp. Phys. **134**, 269 (2004).
[23] F. Paesani, R.E. Zillich, Y. Kwon, and K.B. Whaley, J. Chem. Phys. **122**, 181106 (2005).
[24] A.R.W. McKellar, J. Chem. Phys. **92**, 3261 (1990).
[25] L.S. Costa and D.C. Clary, J. Chem. Phys. **117**, 7512 (2002).
[26] G. Tejeda, J.M. Fernández, S. Montero, D. Blume, and J.P. Toennies, Phys. Rev. Lett. **92**, 223401 (2004).

[27] M.D. Brookes, C. Xia, J. Tang, J.A. Anstey, B.G. Fulsom, K.-X. Au Yong, J.M. King, and A.R.W. McKellar, Spectrochim. Acta A **60**, 3235 (2004).

[28] X.-G. Wang, T. Carrington, Jr., J. Tang, and A.R.W. McKellar, J. Chem. Phys., in press.

[29] A.R.W. McKellar, J. Chem. Phys. **122**, 174313 (2005).

Table I. Assigned transitions for (*para*H_2)$_N$-OCS clusters (in cm^{-1}).

N	*P*(2)	*P*(1)	*R*(0)	*R*(1)	*R*(2)
2	2223.0960	2223.6494	2224.7718	2225.3207	
3	2223.5202	2223.9847	2224.9421	2225.4031	2225.840[a]
4	2223.9196	2224.3254[b]	2225.1329	2225.5335	2225.9293[a]
5	2224.0992	2224.4473	2225.1396	2225.4832	2225.840[a]
6		2224.3254[b]	2224.8355	2225.0917	2225.3464
7		2224.2083	2224.6353	2224.8477	2225.0570
8		2224.1142	2224.4795	2224.6615	
9		2223.9977	2224.3278[b]	2224.5000	
10		2223.8900	2224.1914	2224.3400	
11		2223.7810	2224.0583	2224.1914[c]	
12		2223.5792[d]	2223.8333		
13		2223.3450[d]	2223.5792	2223.6929[d]	

[a] Not included in fit.

[b] Note that 4 *P*(1), 6 *P*(1) and 9 R(0) overlap (see text).

[c] Coincident with 10 *R*(0).

[d] These assignments are less certain (see text).

Table II. Assigned transitions for (*ortho*H_2)$_N$-N_2O clusters (in cm^{-1}).

N	*P*(2)	*P*(1)	*Q*(*J*)	*R*(0)	*R*(1)	*R*(2)
2		2224.4756	2224.99	2225.5369	2226.0512	
3	2224.7737[a]	2225.2130	2225.6532	2226.0970	2226.5302	2226.9511
4	2224.5493[a]	2225.9233	2226.2920	2226.6643	b	2227.3929
5	2225.9605	c	2226.5833	2226.8952	2227.2032	2227.5094
6			2226.6053	2226.8426	2227.0756	
7				2226.6466	2226.8290	2227.0188

[a] Not included in fit.

[b] Obscured by the N_2O *R*(3) line.

[c] Obscured by the 4 *Q* line

Table III. $R(0)$ transitions of mixed $(para\text{-}H_2)_N$ - $(ortho\text{-}H_2)_M$ - N_2O clusters (in cm^{-1}).[a]

$N+M$	N	M	Observed $R(0)$	Predicted $R(0)$ [a]
2	1	1	2225.154	2225.154
3	2	1	2225.326[b]	2225.327
3	1	2	2225.710	2225.712
4	3	1	2225.518	2225.516
4	2	2	2225.902	2225.899
4	1	3	2226.284[c]	2226.281
5	4	1	2225.503	2225.491
5	3	2	2225.862	2225.842
5	2	3	2226.214	2226.193
5	1	4	2226.557	2226.544

[a] Predicted by linear interpolation between the observed $R(0)$ lines of the corresponding pure clusters of the same size ($N + M$).

[b] Partly obscured by a $para\text{-}H_2\text{-}N_2O$ line.

[c] Partly obscured by the $(ortho\text{-}H_2)_4\text{-}N_2O$ Q feature.

Table IV. Linear molecule analyses of the infrared transitions of $(H_2)_N$–N_2O clusters (values in cm^{-1}).[a]

N	hydrogen	ν_0	*B*’	*B*”	*D*” = *D*’
2	*para*H_2	2224.2102	0.2803	0.2817	0.19×10^{-3}
3	*para*H_2	2224.4625	0.2407 [b]	0.2407	0.66×10^{-3}
4	*para*H_2	2224.7279	0.2019 [b]	0.2019	0.02×10^{-3}
5	*para*H_2	2224.7923	0.1731 [b]	0.1731	0.01×10^{-3}
6	*para*H_2	2224.5806	0.1277 [b]	0.1277	0.00×10^{-3}
7	*para*H_2	2224.4218	0.1069 [b]	0.1069	0.06×10^{-3}
8	*para*H_2	2224.2969	0.0914 [b]	0.0914	0.03×10^{-3}
9	*para*H_2	2224.1628	0.0819 [b]	0.0819	-0.30×10^{-3}
10	*para*H_2	2224.0407	0.0755 [b]	0.0755	0.09×10^{-3}
11	*para*H_2	2223.9197	0.0695 [b]	0.0695	0.07×10^{-3} [c]
12	*para*H_2	2223.7063	0.0637 [b]	0.0637	0.07×10^{-3} [c]
13	*para*H_2	2223.4621	0.0588 [b]	0.0588	0.14×10^{-3}
2	*ortho*H_2	2225.0076	0.2657[a]	0.2670	0.51×10^{-3}
3	*ortho*H_2	2225.6539	0.2217	0.2212	0.33×10^{-3}
4	*ortho*H_2	2226.2920	0.1867	0.1849	0.28×10^{-3}
5	*ortho*H_2	2226.5826	0.1562 [b]	0.1562	0.10×10^{-3}
6	*ortho*H_2	2226.6053	0.1190 [b]	0.1190	0.18×10^{-3}
7	*ortho*H_2	2226.4544	0.0965 [b]	0.0965	0.20×10^{-3} [c]

[a] *B*’ was constrained to equal 0.995 x *B*”.

[b] *B*’ was constrained to equal *B*”.

[c] *D* was constrained to this value.

FIGURE CAPTIONS

Fig. 1. Observed infrared spectra of (*para*H_2)$_N$-N_2O clusters. Digits preceding the rotational assignments give the cluster size, N, so that 3 $R(0)$ is the $J = 1 \leftarrow 0$ transition of (*para*H_2)$_3$-N_2O. The top 3 traces are taken with a pinhole jet nozzle, and the bottom 3 with a slit nozzle; within these groups the traces are arranged from bottom to top in order of increasing backing pressure. The symbol 1# indicates a line of *ortho*H_2-N_2O, and 'm' indicates a mixed (*para*H_2/*ortho*H_2) cluster (see text).

Fig. 2. Observed infrared spectra of larger (*para*H_2)$_N$-N_2O clusters in the wavenumber region immediately below that of Fig. 1. Backing pressure and nozzle temperature are shown beneath each trace.

Fig. 3. Observed infrared spectra of even larger (*para*H_2)$_N$-N_2O clusters.

Fig. 4. Observed infrared spectra of (*ortho*H_2)$_N$-N_2O clusters, obtained using normal H_2 in the expansion gas mixture. The symbol 'm' indicates a mixed cluster (see text).

Fig. 5. Observed dependence of the vibrational band origin on cluster size for (*para*H_2)$_N$-N_2O and (*ortho*H_2)$_N$-N_2O clusters, with previous results for (He)$_N$-N_2O shown for comparison. Note the initial blue shifts for $N = 0$ to 5 (6 for *ortho*H_2), followed by a turnaround to a red shift.

Fig. 6. Observed dependence of the rotational constant, B, on cluster size for (*para*H_2)$_N$-N_2O and (*ortho*H_2)$_N$-N_2O clusters. Note the slightly larger than expected value for $N = 5$ reflecting the compact size of this cluster.

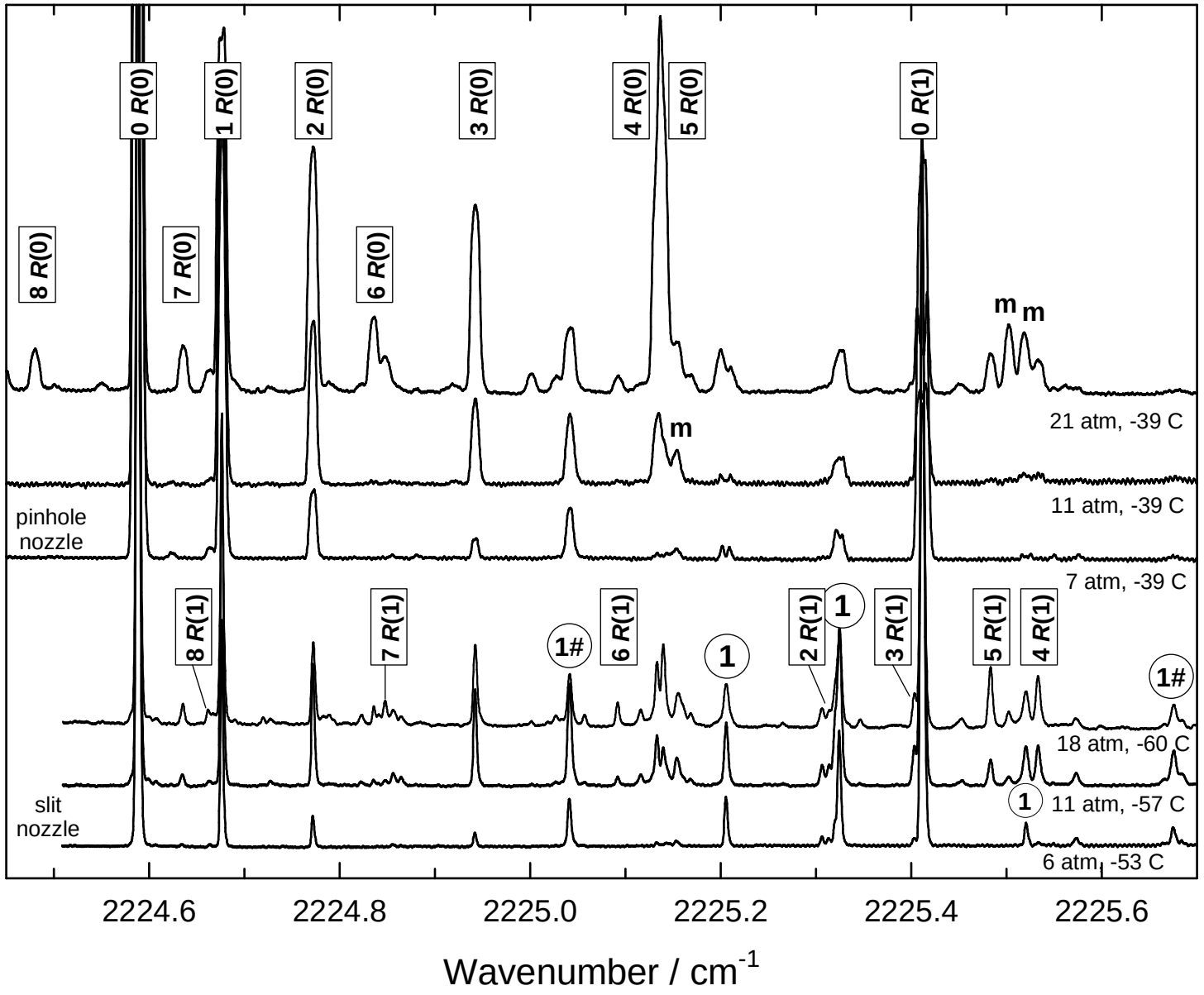
0 R(0)
1 R(0)
2 R(0)
3 R(0)
4 R(0)
5 R(0)
0 R(1)
8 R(0)
7 R(0)
6 R(0)
m
m
m
21 atm, -39 C
11 atm, -39 C
pinhole
nozzle
7 atm, -39 C
8 R(1)
7 R(1)
1#
6 R(1)
1
2 R(1)
1
3 R(1)
5 R(1)
4 R(1)
1#
18 atm, -60 C
1
11 atm, -57 C
slit
nozzle
6 atm, -53 C
2224.6
2224.8
2225.0
2225.2
2225.4
2225.6
Wavenumber / cm-1

Figure 1.

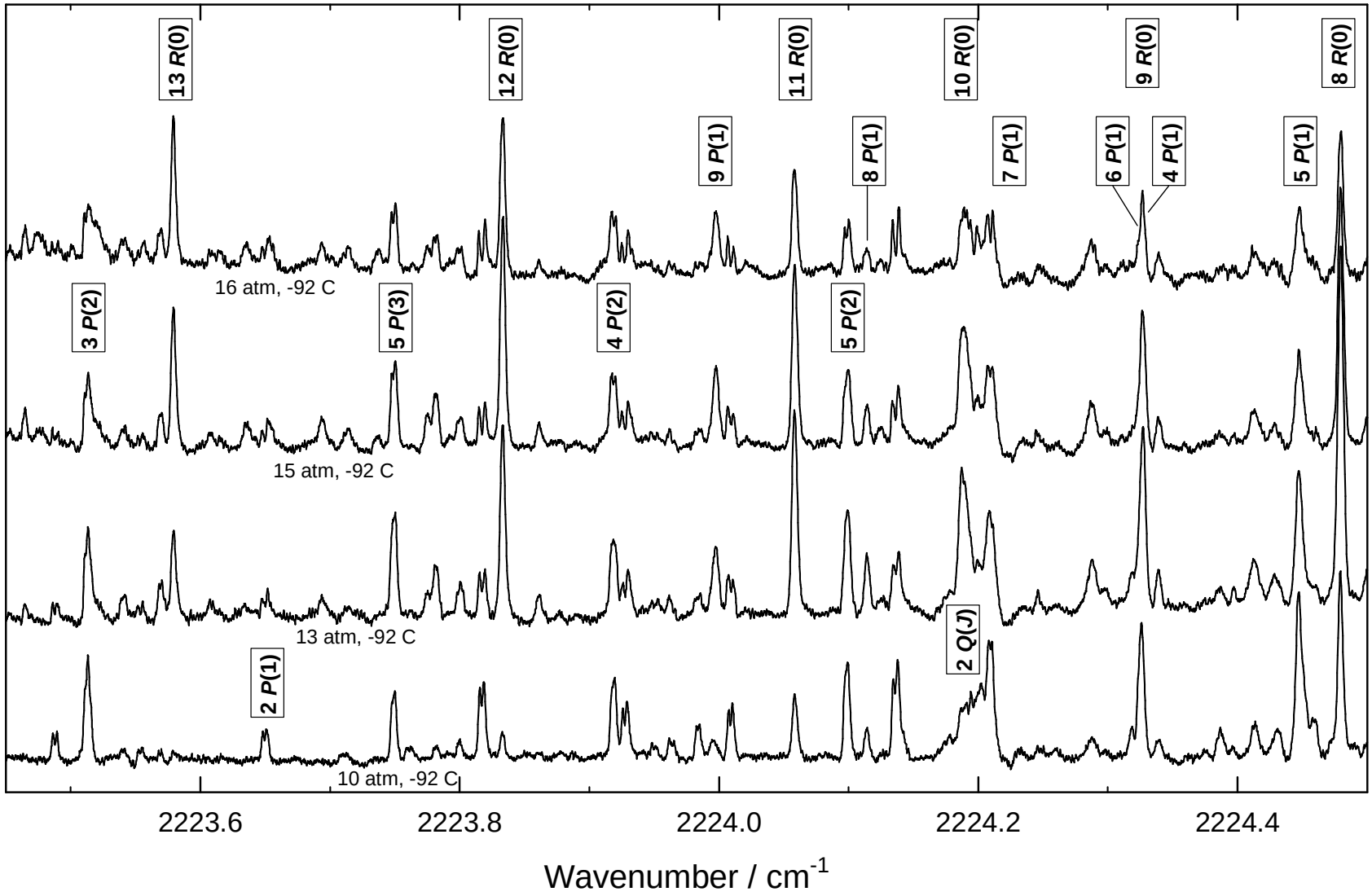
13 R(0)
12 R(0)
11 R(0)
10 R(0)
9 R(0)
8 R(0)
9 P(1)
8 P(1)
7 P(1)
6 P(1)
4 P(1)
5 P(1)
16 atm, -92 C
3 P(2)
5 P(3)
4 P(2)
5 P(2)
15 atm, -92 C
13 atm, -92 C
2 P(1)
2 Q(J)
10 atm, -92 C
2223.6
2223.8
2224.0
2224.2
2224.4
Wavenumber / cm-1

Figure 2.

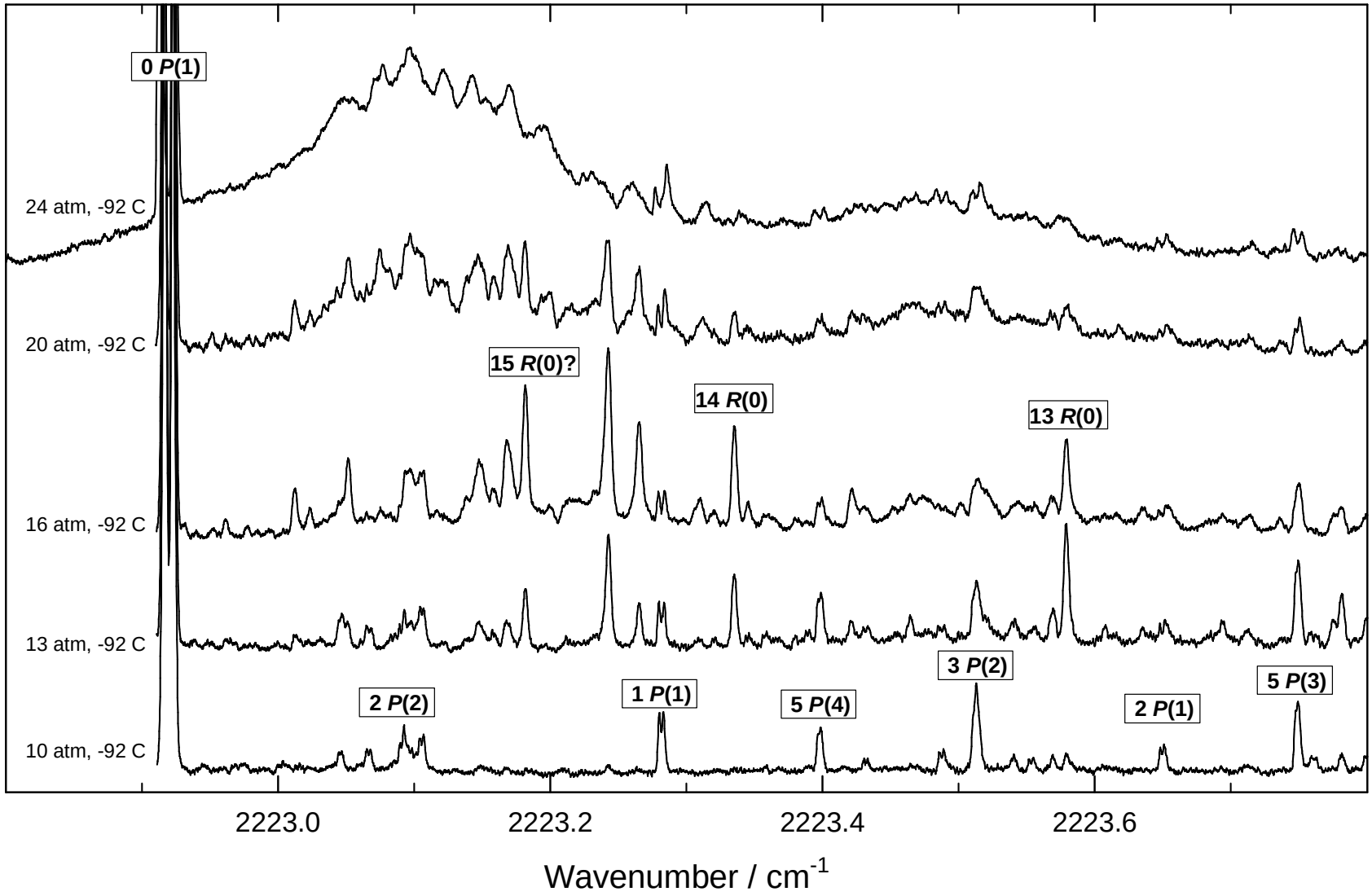
0 P(1)
24 atm, -92 C
20 atm, -92 C
15 R(0)?
14 R(0)
13 R(0)
16 atm, -92 C
13 atm, -92 C
3 P(2)
5 P(3)
2 P(2)
1 P(1)
5 P(4)
2 P(1)
10 atm, -92 C
2223.0
2223.2
2223.4
2223.6
Wavenumber / cm-1

Figure 3.

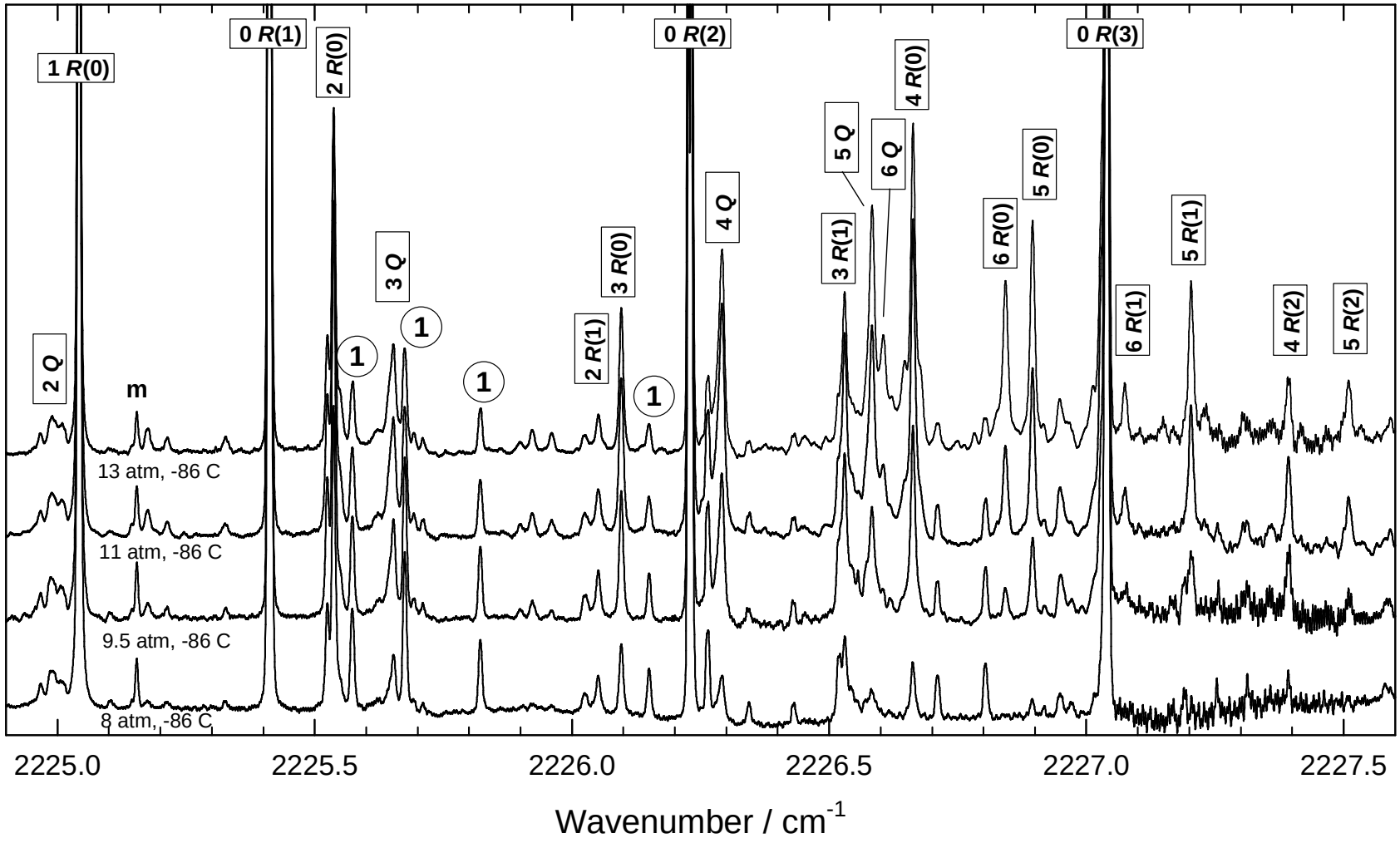
1 R(0)
0 R(1)
2 R(0)
0 R(2)
0 R(3)
2 Q
m
3 Q
1
1
1
2 R(1)
3 R(0)
1
4 Q
5 Q
3 R(1)
6 Q
4 R(0)
6 R(0)
5 R(0)
6 R(1)
5 R(1)
4 R(2)
5 R(2)
13 atm, -86 C
11 atm, -86 C
9.5 atm, -86 C
8 atm, -86 C
2225.0
2225.5
2226.0
2226.5
2227.0
2227.5
Wavenumber / cm-1

Figure 4.

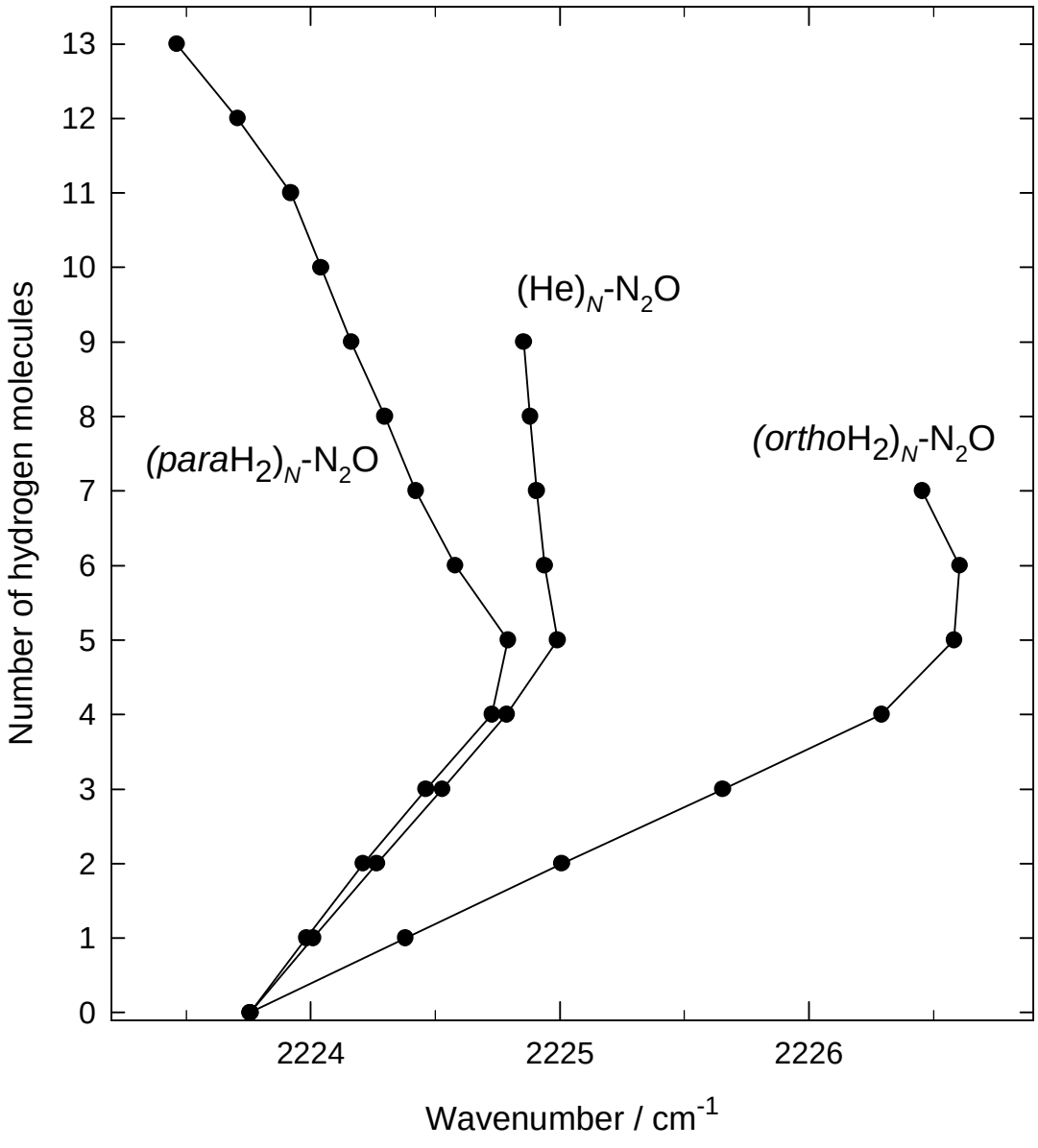
Number of hydrogen molecules
Wavenumber / cm-1
(He)N-N2O
(paraH2)N-N2O
(orthoH2)N-N2O
0
1
2
3
4
5
6
7
8
9
10
11
12
13
2224
2225
2226

Figure 5.

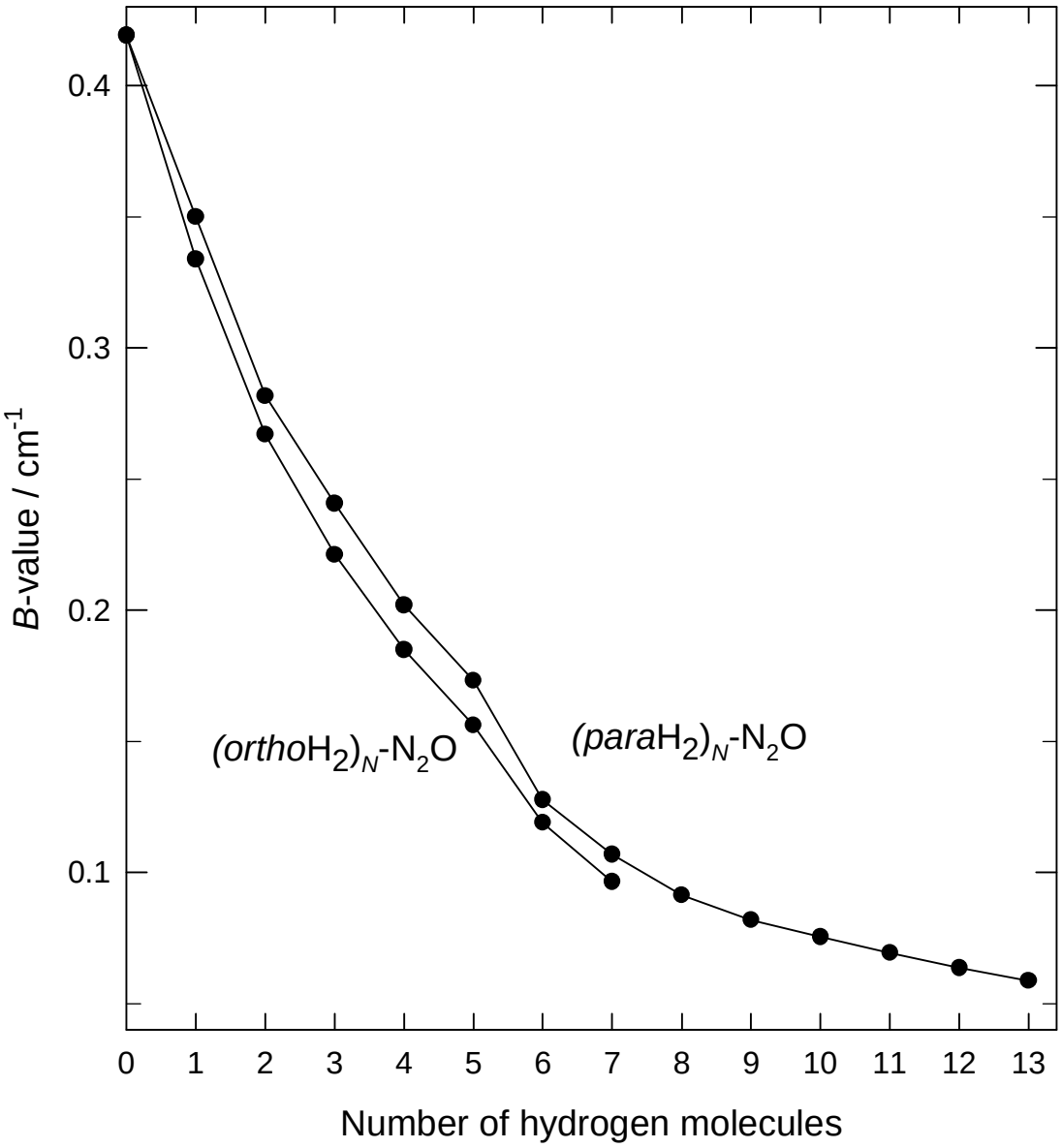
0.4
0.3
0.2
0.1
B-value / cm-1
(orthoH2)N-N2O
(paraH2)N-N2O
0
1
2
3
4
5
6
7
8
9
10
11
12
13
Number of hydrogen molecules

Figure 6.